OPEN

Selective and Recyclable Congo Red Dye Adsorption by Spherical Fe_3O_4 Nanoparticles Functionalized with 1,2,4,5-Benzenetetracarboxylic Acid

Sobhan Chatterjee[1], Nikita Guha[2], Sarathkumar Krishnan[2], Amrendra K. Singh[1], Pradeep Mathur[1] & Dhirendra K. Rai[2]*

In this study, the new material Fe_3O_4@BTCA has been synthesized by immobilization of 1,2,4,5-Benzenetetracarboxylic acid (BTCA) on the surface of Fe_3O_4 NPs, obtained by co-precipitation of $FeCl_3.6H_2O$ and $FeCl_2.4H_2O$ in the basic conditions. Characterization by P-XRD, FE-SEM, and TEM confirm Fe_3O_4 has a spherical crystalline structure with an average diameter of 15 nm, which after functionalization with BTCA, increases to 20 nm. Functionalization also enhances the surface area and surface charge of the material, confirmed by BET and zeta potential analyses, respectively. The dye adsorption capacity of Fe_3O_4@BTCA has been investigated for three common dyes; Congo red (C.R), Methylene blue (M.B), and Crystal violet (C.V). The adsorption studies show that the material rapidly and selectively adsorbs C.R dye with very high adsorption capacity (630 mg/g), which is attributed to strong H-bonding ability of BTCA with C.R dye as indicated by adsorption mechanism study. The material also shows excellent recyclability without any considerable loss of adsorption capacity. Adsorption isotherm and kinetic studies suggest that the adsorption occurs by the Langmuir adsorption model following pseudo-second-order adsorption kinetics.

Organic dyes are one of the significant contributors to water pollution caused by the discharge of effluent from various industries such as textile, plastic, printing, photographic, paper-pulp, paint, and leather[1–9]. There are many techniques for wastewater treatment, for instance, coagulation, electrocoagulation, chlorination, ozonation, flotation, chemical oxidation, filtration, membrane separation, adsorption, and ultrafiltration[10–17]. Among various reported techniques, the adsorption is the most convenient and well-established technique because of high efficiency, simplicity, and minimum energy requirement[18–24].

In recent times, porous metal oxides have been recognized as excellent solid adsorbents for wastewater treatment owing to their high surface area and the presence of sufficient active surface sites[25–28]. Among various metal oxides, Fe_3O_4 nanoparticles (NPs) are drawing considerable attention due to their unique properties such as excellent biocompatibility, low synthetic cost, ease of functionalization, and high magnetic susceptibility leading to easy magnetic recovery[29–34]. Owing to the negatively charged surface, bare Fe_3O_4 NPs have been shown as dye absorbents in many reports[35–37]; however, its applicability is limited due to low adsorption capacity and poor selectivity and recyclability. Chaudhary et al. have reported the use of Fe_3O_4 NPs for adsorption of acridine orange dye, Coomassie brilliant blue R-200 dye, and Congo red dye[37]. Jia et al. developed 3D hierarchical porous Fe_3O_4 NPs, which have been used for C.R dye adsorption, however, with low adsorption capacity of 39.10 mg/g[25]. Similarly, hydrothermal preparation of Fe_3O_4 NPs and its application for C.R dye removal from aqueous solution, with adsorption capacity of 28.46 mg/g, has been reported by Wang et al.[35].

Besides electrostatic interactions as applicable to the cases mentioned above, the adsorption of dye is also actively facilitated by hydrogen bonding, which depends on functional groups and active coordination sites

---

[1]Discipline of Chemistry, Indian Institute of Technology Indore, Simrol, Indore, 453552, India. [2]Discipline of Metallurgy Engineering and Materials Science, Indian Institute of Technology Indore, Simrol, Indore, 453552, India. *email: dkrai@iiti.ac.in
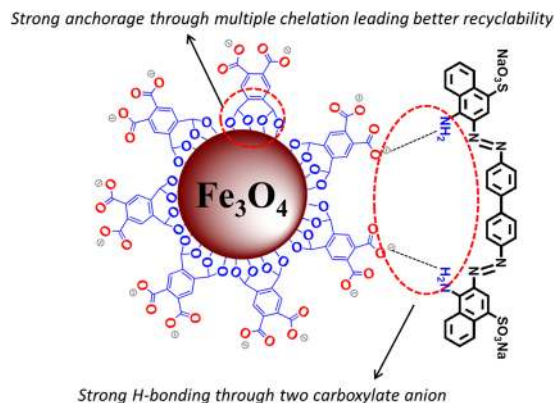
1

Figure 1. Schematic illustration of Fe_3O_4@BTCA material adsorption towards Congo red dye through H-bonding carboxylate anions.

present on the solid surface. Thus, to achieve higher adsorption capacity, many researchers have focused their efforts on the functionalization of the Fe_3O_4 surface by introducing organic chelate groups[38–42] and metal oxide[43–47]. For example, polyaniline (PANI) and carbon nanotube (CNT) functionalized Fe_3O_4 NPs were reported by Zhao *et al.*, which showed a moderate value of adsorption capacity (417.38 mg/g)[40]. Wang *et al.* reported polyethyleneimine/graphene oxide/Fe_3O_4 based nanocomposite material with 574.7 mg/g adsorption capacity[38].

In the present work, we have explored a multi carboxylate organic ligand 1,2,4,5-Benzentetracarboxylic acid (BTCA) for surface functionalization of Fe_3O_4 nanoparticles for rapid and selective adsorption of a ubiquitous industrial pollutant Congo red dye. Though there are many reports on surface functionalization with carboxylate groups[48–50], BTCA group, containing four carboxylate groups at 1, 2, 4 and 5- positions of the benzene ring as functionalization agent, is expected to significantly improve the adsorption capacity for selective dyes with better recyclability as illustrated in Fig. 1. Formation of two covalent bonds, in chelate fashion, by condensation of two –COOH groups from BTCA and two –OH groups from Fe_3O_4 surface will cause a firm anchorage of BTCA on Fe_3O_4 surface. The remaining two –COO$^-$ groups, formed under synthetic conditions, can form a strong H-bonding with a primary amine-containing dye, like Congo red, which will lead to high adsorption capacity. To best of our knowledge, it is the first report where BTCA has been employed as a surface functionalization ligand for any material.

The present report discusses the synthesis and characterization of BTCA functionalized Fe_3O_4 NPs (Fe_3O_4@BTCA), which rapidly and selectively adsorbs a primary amine-containing Congo red dye from its aqueous solution. The adsorption studies show that Fe_3O_4@BTCA material exhibits significantly higher adsorption capacity and can be reused in multiple cycles without undergoing any considerable loss in adsorption performance. Mechanisms for selective adsorption and adsorption kinetics have also been described.

Results and Discussion

The synthetic steps involved in the preparation of Fe_3O_4 and subsequent immobilization of BTCA groups to obtain Fe_3O_4@BTCA is depicted in Fig. 2. To confirm the formation of Fe_3O_4 and Fe_3O_4@BTCA materials (Fig. 3), Fourier transform infrared spectroscopy (FT-IR), Thermo-gravimetric analysis (TGA) and Powder X-ray diffraction (PXRD), and for structural confirmation, BET surface area analysis, Scanning electron microscopy (SEM) and Transmission electron microscopy (TEM) analyses were performed.

The FT-IR spectra of Fe_3O_4 and Fe_3O_4@BTCA materials are shown in Fig. 3A,B. The characteristic absorption bands for Fe_3O_4 material appear at 585, 635, 1405, 1625, and 3426 cm^{-1}, whereas, for Fe_3O_4@BTCA material, bands appear at 585, 635, 1385, 1491, 1581, 1625, 3426 cm^{-1}. The common peaks at 585 and 635 cm^{-1} can be assigned to Fe-O bond vibrations[52], while broad absorption bands appearing at 1625, 1405, and 3426 cm^{-1} arise due to O-H bond vibration of water molecules[53–55] adsorbed on the surface of both materials. The appearance of additional peaks at 1385, 1491 and 1581 cm^{-1} in the case of Fe_3O_4@BTCA indicates the presence of BTCA group. Among these new peaks, the peak at 1581 cm^{-1} can be attributed to asymmetric C-O stretching of carboxylate groups, while the peaks at 1491 and 1485 cm^{-1} are due to aromatic C = C bond vibrations of benzene and the symmetric stretching of carboxylate groups, respectively[56]. Further to ensure the functionalization of BTCA on to the Fe_3O_4 surface, UV-Vis spectrum of aqueous BTCA solution was compared with that of aqueous Fe_3O_4@BTCA suspension (Fig. 3C). The absorption peak at 220 nm of BTCA was found shifted to 211 nm in Fe_3O_4@BTCA, indicating presence of BTCA on the Fe_3O_4 surface in deprotonated form[57].

The TGA curves for Fe_3O_4 and Fe_3O_4@BTCA are depicted in Fig. 3D. Both materials show an initial small weight loss at temperatures below 200 °C due to desorption of adsorbed water molecules onto their surfaces. The higher weight percentage loss in the case of Fe_3O_4@BTCA (2.50%) compared to Fe_3O_4 (1.07%) indicates more water adsorbed on Fe_3O_4@BTCA due to stronger hydrogen bonding facilitated by the presence of free carboxylate groups. The second region showing 7.01% weight loss in Fe_3O_4@BTCA compared to 1.51% in Fe_3O_4 indicates the presence of higher organic contents (BTCA) in the case of former. As expected, both materials show similar thermal decomposition behavior beyond 500 °C. Overall, a comparison of three decomposition segments in both materials hints a successful grafting of BTCA group on to the surface of Fe_3O_4. Presence of BTCA group on to the
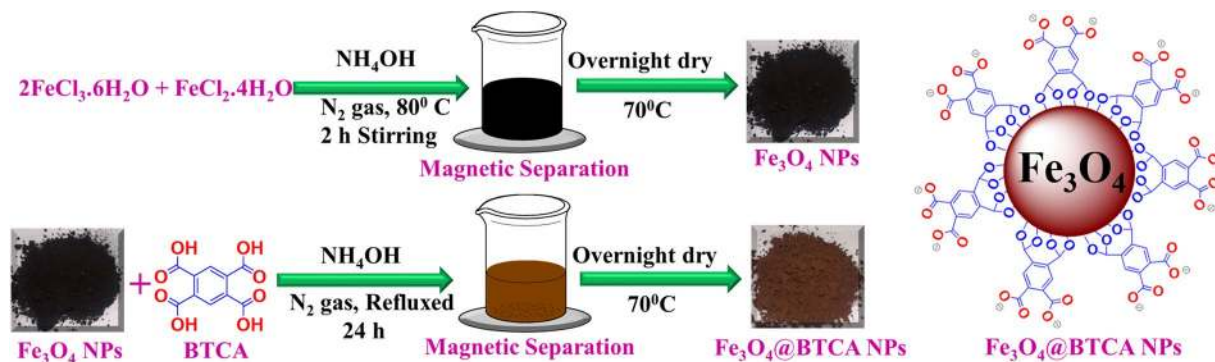
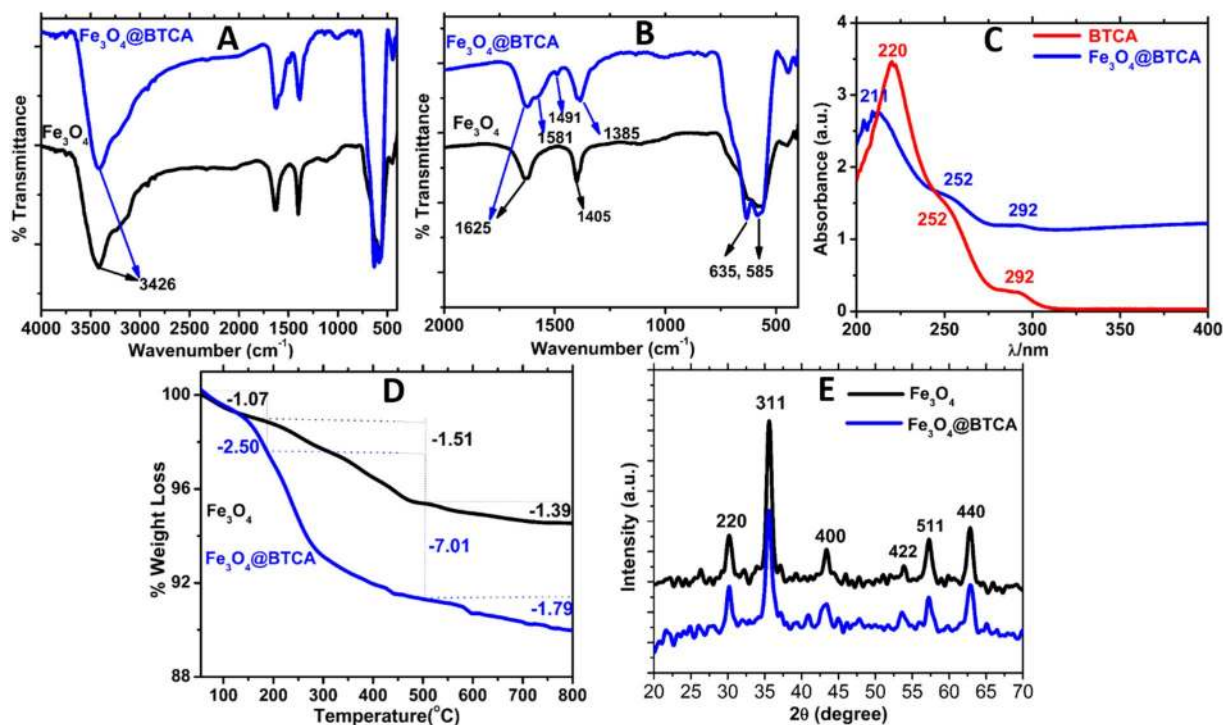**Figure 2.** Schematic illustration of the preparation of surface-modified Fe_3O_4@BTCA.

Figure 3. (**A**) FT-IR spectra of Fe_3O_4 and Fe_3O_4@BTCA, (**B**) FT-IR for shorter range, (**C**) UV-Vis spectra of BTCA and Fe_3O_4@BTCA, (**D**) TGA and (**E**) PXRD pattern of Fe_3O_4 and Fe_3O_4@BTCA.

surface of Fe_3O_4 in Fe_3O_4@BTCA is also supported by its EDX spectrum, where peak corresponding to carbon can be clearly seen (Figure S1 in ESI).

The structural information was verified by the powder X-ray diffraction (PXRD) technique. The powder X-ray diffraction patterns of both materials are illustrated in Fig. 3E. Both materials have six characteristic peaks at $2\theta = 30.18$, 35.49, 43.30, 53.77, 57.21, and 62.83 which correspond to the (220), (311), (400), (422), (511), and (440) reflection planes, respectively, of an fcc magnetite. The crystalline structure of these materials can be established with the standard pattern of Fe_3O_4 (ICDD card No 19-0629), which supports that both materials have a pure Fe_3O_4 phase with a spinel structure. As evident from the diffraction pattern, immobilization of the BTCA group does not change the Fe_3O_4 phase. Using Scherrer equation on PXRD line broadening, the calculated average particle size of Fe_3O_4 is found to be 12 nm. The (311) plane mean diffraction peak at $2\theta = 35.49$ was used to determine the particle size because of its intense nature.

TEM images of as-synthesized Fe_3O_4, Fe_3O_4@BTCA, and Congo Red dye loaded species (Fe_3O_4@BTCA@C.R) are shown in Fig. 4A–D. As observed from the TEM images, the spherical shape of the particles is quite evident for all three materials, which is also observed in the SEM images of Fe_3O_4 and Fe_3O_4@BTCA (Fig. 4E,F). The estimated mean diameter for the Fe_3O_4 particle is 10–15 nm (Fig. 4A), which compares well with that obtained from PXRD, and increases to 20 nm after functionalization with BTCA (Fig. 4C). In the HRTEM of Fe_3O_4, the 311 planes of spherical Fe_3O_4 can be clearly seen with an inter-planar distance of 0.266 nm (Fig. 4B).
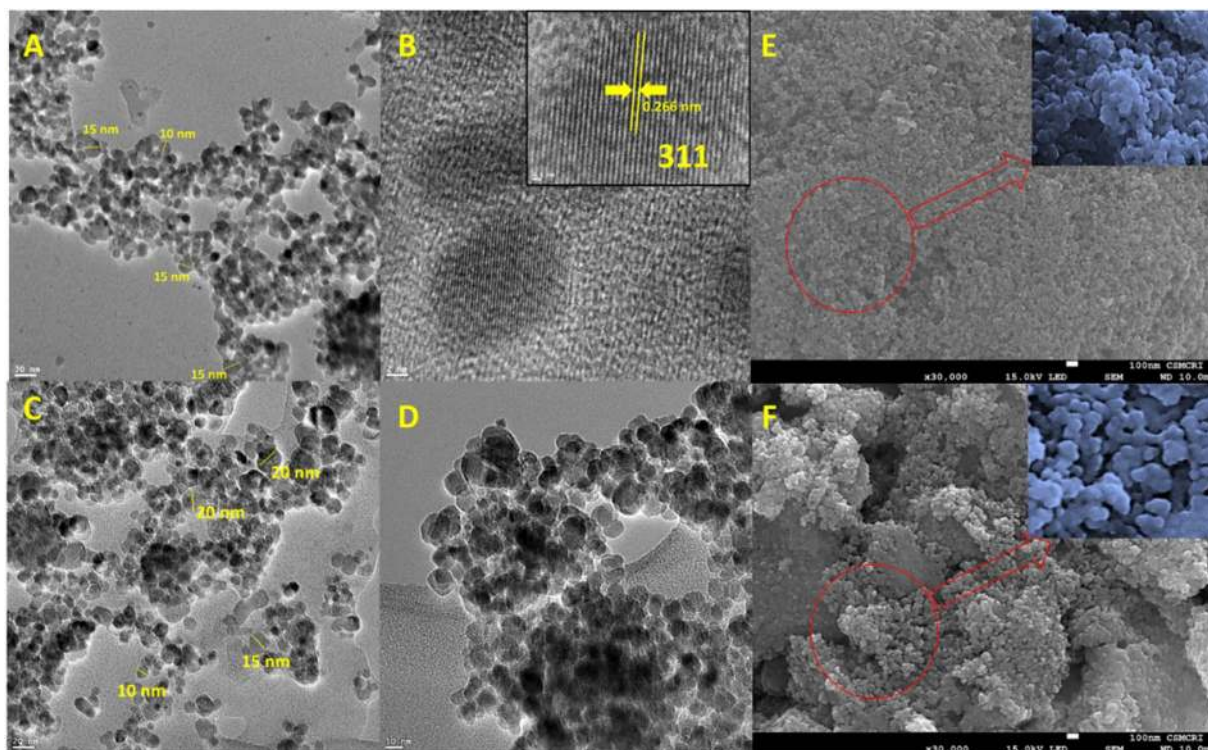
Figure 4. TEM images of (**A**) Fe_3O_4, (**B**) Fe_3O_4 (HRTEM), (**C**) Fe_3O_4@BTCA, (**D**) Fe_3O_4@BTCA@C.R. SEM images of (**E**) Fe_3O_4 and (**F**) Fe_3O_4@BTCA.

The porous structures of as-synthesized Fe_3O_4 and Fe_3O_4@BTCA were analyzed by N_2 adsorption-desorption isotherm using a multipoint BET method within the relative pressure (P/Po) range of 0.05–1 (Figure S2A), and by BJH pore size distribution analysis (Figure S2B). The pore sizes, pore volumes, and BET surface areas of both materials are tabulated in Table S1 in ESI. Both materials exhibit type IV isotherms with H3hysteresis loops at relatively high pressure region P/Po = 0.8–1. BJH pore size distribution shows that the surface functionalization by BTCA does not alter any appreciable change in pore size of Fe_3O_4@BTCA (12.31 nm) compared to that of Fe_3O_4 (12.41 nm). This indicates that the immobilization of BTCA occurs on the outer surface of Fe_3O_4. The enhanced surface area of Fe_3O_4@BTCA (72.35 m^2/g) compared to that of Fe_3O_4 (46.66 m^2/g) can be attributed to a higher dispersity of Fe_3O_4@BTCA NPs due to negatively charged surface repulsion.

Surface charge analyses by zeta-potential calculations of Fe_3O_4 and Fe_3O_4@BTCA show that the former, having −7.21 mV potential, possess significantly lesser negative surface charge than the later having −17.8 mV. Observation of the higher negative surface charge in the case of Fe_3O_4@BTCA is understandable as it bears BTCA groups with a number of free carboxylate groups covering the surface. For Fe_3O_4@BTCA, information about the higher surface area from BET and the idea of greater negative surface charge from surface charge analysis together support our assumption of obtaining better adsorption efficiency by immobilization of BTCA groups.

As the surface of Fe_3O_4@BTCA bears free carboxylate groups, reprotonation and de-protonation are expected to affect its surface charge. Therefore, the surface charge analysis of Fe_3O_4@BTCA was carried out at various pH, and the calculated zeta-potentials at different pH are shown in Fig. S3 in ESI. Due to excess protonation, the calculated zeta-potential is in the positive range till pH 5, whereas, an increasing trend of the negative surface is observed upon increasing pH above 5 because of deprotonation of –COOH groups on the surface. This observation supports our proposed mechanism of dye adsorption onto the Fe_3O_4@BTCA surface, as discussed later.

The ability of Fe_3O_4@BTCA to adsorb dyes on to its surface, leading to the color removal of aqueous dye solutions was investigated towards C.R (Congo red), M.O (Methyl Orange), and C.V (Crystal Violet) by UV-Vis absorption spectroscopy. Figure 5 shows the color removal of aqueous dye solutions of C.R, M.O, and C.V before and after shaking the solution with Fe_3O_4@BTCA for 15 minutes. It is evident that Fe_3O_4@BTCA does selective adsorption of C.R dye leading to 97% color removal (Fig. 5A). However, in the case of M.O and C.V, only 14% and 9% color removal, respectively, were observed under similar adsorption conditions, suggesting no considerable absorption of M.O and C.V (Fig. 5B,C). UV-Vis spectra also indicate that the two intense absorption peaks of C.R at 338 and 498 nm vanish entirely after treatment with Fe_3O_4@BTCA. However, a similar phenomenon for M.O and C.V was not observed as the intensities of their UV-Vis absorption peaks remain almost unaltered after treatment with Fe_3O_4@BTCA. We also investigated similar color removal studies for C.R by as-synthesized Fe_3O_4 NPs, which indicate only 12% color removal (Fig. S4 in ESI). To reach an optimum condition for C.R dye adsorption, its color removal studies were performed at different dye concentrations (20–100 ppm), Fe_3O_4@BTCA doses (5 and 15 mg), and pH conditions (2–10). The resulting graph and bar diagram with corresponding values are given in Fig. S5 in ESI. An increasing percentage color removal trend was observed upon increasing the pH of the
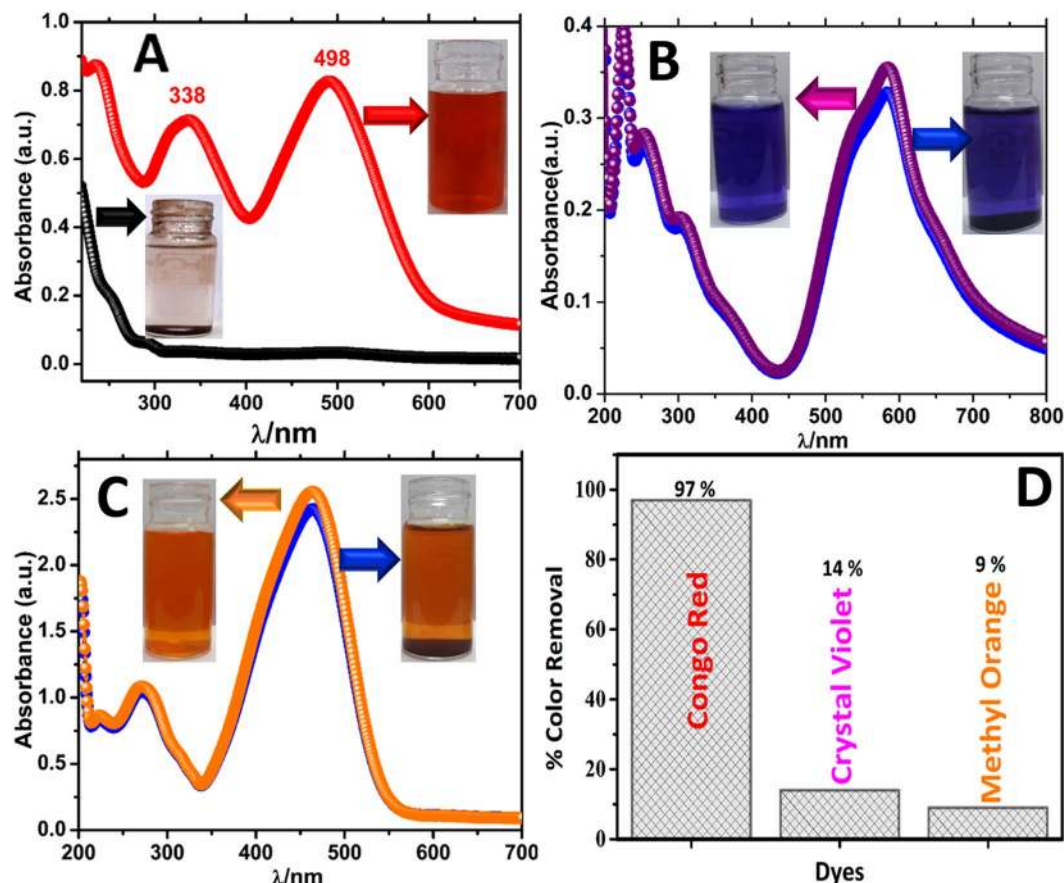
Figure 5. UV-Vis spectra of (**A**) C.R dye, (**B**) C.V dye, (**C**) M.O dye aqueous solutions before and after shaking with Fe_3O_4@BTCA, (**D**) Bar diagram for percentage removal of C.R, C.V, and M.O dyes (percentage color removal $= 100 \times (C_i-C_f)/C_i$, C_i and C_f are concentrations of dyes before and after shaking with Fe_3O_4@BTCA, respectively).

solution until pH 7 (97% color removal), which remains constant after further increase in pH. Best adsorption in terms of percentage color removal (97%) was observed with 20 mg catalyst dose in 20 ppm solution of C.R dye.

Further to support the fact that the color removal of Congo red dye is caused by its adsorption on to the surface of Fe_3O_4@BTCA, using FT-IR and UV-Vis spectroscopy, we also ensured the formation of Fe_3O_4@ BTCA@C.R species containing adsorbed C.R dye on the surface of Fe_3O_4@BTCA. Fe_3O_4@BTCA@C.R was obtained by stirring 50 mg of Fe_3O_4@BTCA in 100 ppm aqueous solution of C.R dye for 15 minutes, followed by its magnetic separation, washing and drying at 70 °C for 24 h. The UV-Vis absorption spectrum of this material shows two weak peaks at 498 and 338 nm (Fig. S6 in ESI), indicating the presence of C.R dye on the surface of Fe_3O_4@BTCA material. The same is also supported by FT-IR spectrum (Fig. S7 in ESI), in which appearance of a peak at 1047 cm^{-1} is due to vibration of S=O group present in C.R dye[28].

In order to estimate the adsorption capacity of Fe_3O_4@BTCA towards C.R dye and to understand the adsorption behavior (Langmuir type or Freundlich type), adsorption isotherm studies were performed through batch experiments. Prior to the adsorption study, a calibration plot (Fig. S8 in ESI) of concentration versus absorbance was drawn by recording UV-Vis spectra of aqueous C.R dye solutions of different concentrations. Adsorption study was performed by allowing adsorption of 10 batches of 50 mL aqueous C.R dye solutions of varying concentrations (10–100 ppm) on a fixed amount of Fe_3O_4@BTCA material (5 mg) through vigorous shaking for 15 minutes. After completion of adsorption, the equilibrium concentration of C.R dye in each magnetically separated filtrate was calculated by comparing its UV-Vis spectrum with the calibration plot. The equilibrium adsorption capacity (q_e) for each batch adsorption can be calculated using Eq. 1 [58–61].

$$q_e = (C_i - C_e)V/W \tag{1}$$

Where C_i and C_e are initial and equilibrium concentrations (mg/L) of C.R dye, respectively. V is the volume of C.R solution (50×10^{-3} L), W is the amount of Fe_3O_4@BTCA (5×10^{-3} g). The adsorption capacity of Fe_3O_4@ BTCA for C.R dye can be estimated from the plot of q_e and C_e values obtained at a different concentration of C.R dye (Fig. 6A). From Fig. 6A, the adsorption capacity of our material towards C.R dye was found to be 630 mg/g, which is significantly higher than the earlier reported Fe_3O_4 based sorbents listed in Table S3 in ESI[38–40,45–47,62–64].
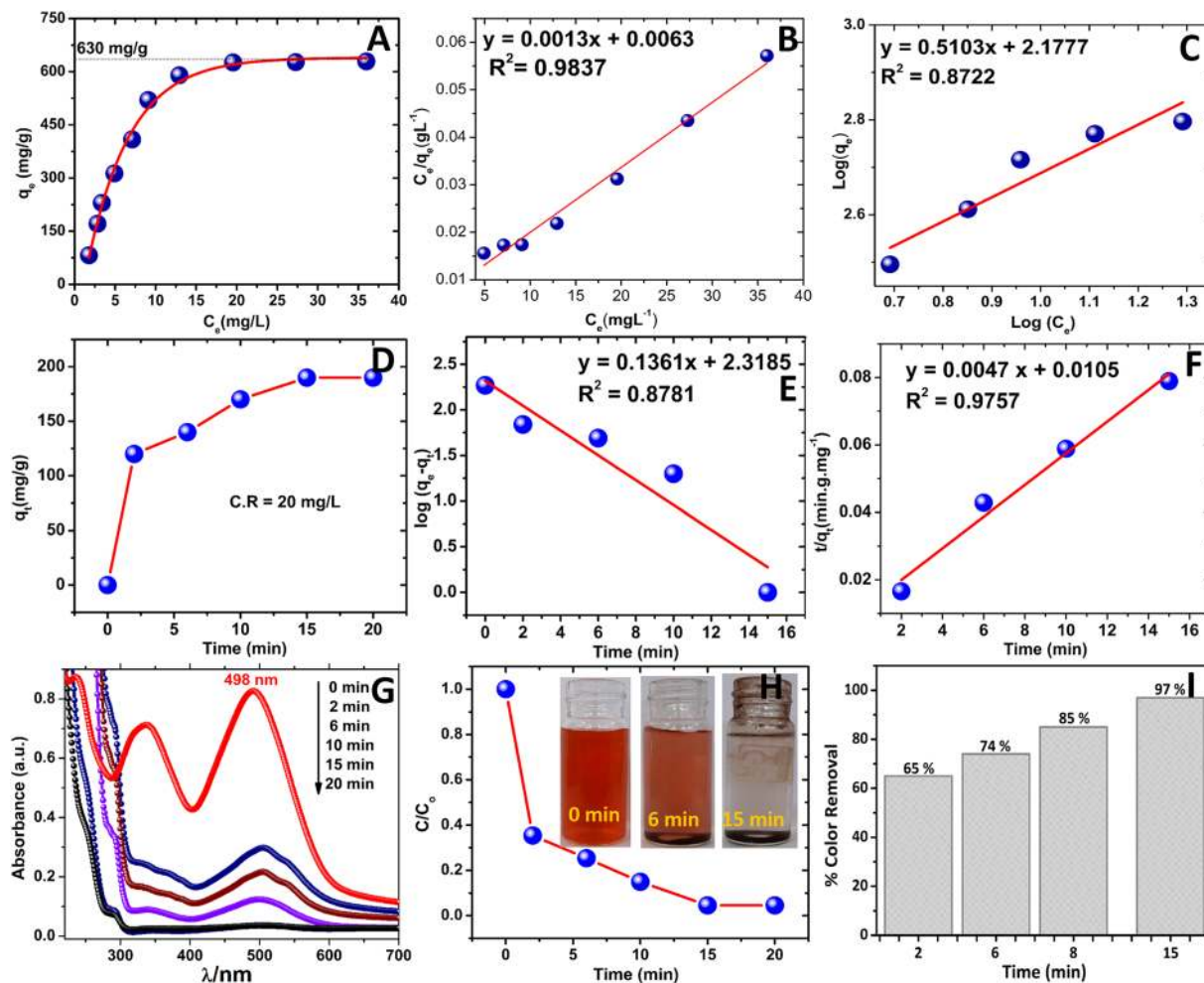
Figure 6. (**A**) Experimental maximum adsorption isotherm of C.R by Fe₃O₄@BTCA, (**B**) Langmuir adsorption isotherm, (**C**) Freundlich adsorption isotherm of C.R dye on Fe₃O₄@BTCA, (**D**) Experimental adsorption capacity with time, (**E**) Pseudo-first-order, (**F**) Pseudo-second-order kinetic plot, (**G**) UV-Vis spectra of C.R dye with increasing time, (**H**) Kinetic plot of C.R dye, (**I**) Percentage color removal of C.R dye with time.

The significantly higher adsorption capacity value for Fe₃O₄@BTCA supports our initial expectations of achieving high adsorption capacity through immobilization of BTCA on the Fe₃O₄ surface by enhancing the surface area and making strong H-binding sites available to promote the dye adsorption.

Adsorption behavior of C.R dye on the surface of Fe₃O₄@BTCA was studied by comparing the fitting of adsorption parameters in the Langmuir and Freundlich type adsorption isotherm equations. Homogeneous monolayer adsorption follows the Langmuir adsorption isotherm given in Eq. 2 [63].

$$\frac{C_e}{q_e}(Langmuir) = \frac{C_e}{q_{max}} + \frac{1}{q_{max} \times K_L} \tag{2}$$

Where C_e and q_e represent the same parameters as mentioned before. q_{max} is adsorption capacity (630 mg/g), and K_L (L/mg) is Langmuir equilibrium constant, which is related to adsorption energy.

The possibility of multilayer adsorption is allowed in the Freundlich adsorption model, and its adsorption isotherm is given in Eq. 3 [64].

$$log q_e(Freundlich) = log K_f + \frac{1}{n} log\ C_e \tag{3}$$

Where K_f and n are Freundlich constants related to adsorption capacity and adsorption intensity, respectively.

From Fig. 6B,C, showing Langmuir and Freundlich isotherms, respectively, it is clear that the experimental adsorption isotherm is best fitting with monolayer Langmuir adsorption isotherm ($R^2 = 0.9837$ for Langmuir and 0.8722 for Freundlich). Other parameters (K_L, q_{max}, K_f, and n) for both adsorption isotherms are given in Table S2A.

In order to understand the adsorption kinetics, the order of the adsorption process was ascertained by fitting the experimental data into the pseudo-first-order and pseudo-second-order equations (Eqs. 4 and 5)[65].
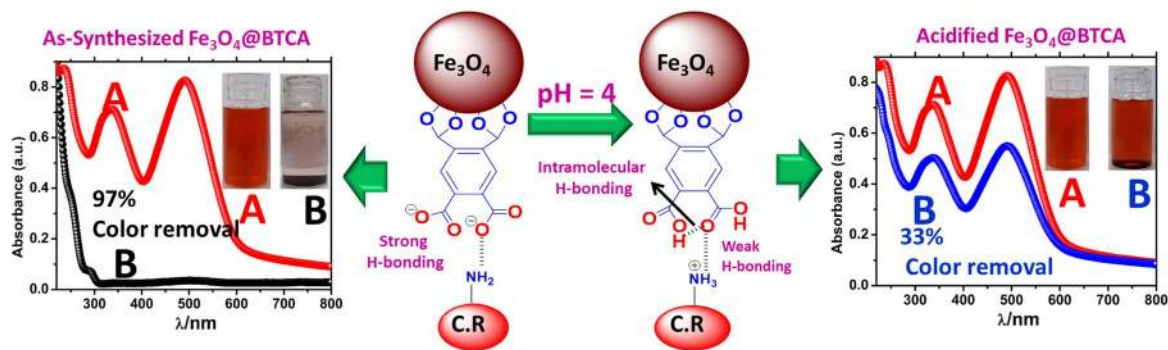
Figure 7. Plausible adsorption mechanism of C.R dye onto Fe_3O_4@BTCA surface.

$$\log(q_e - q_t) = \log q_e - \frac{K_1}{2.303} \times t \tag{4}$$

$$\frac{t}{q_t} = \frac{1}{K_2 \times q_e^2} + \frac{t}{q_e} \tag{5}$$

The equilibrium adsorption capacity (q_t) towards C.R dye was calculated by UV-Vis spectroscopy at different time intervals (t) taking 20 ppm initial aqueous solution of C.R dye with 5 mg Fe_3O_4@BTCA. With increasing time ($t = 2, 6, 8, 15$ and 20 min), the obtained values of q_t are plotted in Fig. 6D. The final value of equilibrium adsorption capacity q_e (192 mg/g) is achieved in 15 min and remains constant with further increase in time interval. Upon fitting the value of q_e (192 mg/g) and that of q_t obtained at a different time interval in straight line Eqs. 4 and 5 (Fig. 6E,F), the best fitting ($R^2 = 0.9757$) was obtained for pseudo-second-order adsorption (remaining kinetic parameters are listed in Table S2B). The extent of color removal with time was also studied under same adsorption conditions. The change in UV-Vis spectra of C.R dye and corresponding percentage change in color upon stirring with Fe_3O_4@BTCA for the different time intervals is given in Fig. 6G. The steep nature of C_o/C vs. time plot (Fig. 6H) suggests rapid dye adsorption up to 2 minutes, which subsequently starts flattening indicating a decrease in the rate of dye adsorption. The bar diagram in Fig. 6I illustrates that within 2 minutes 65% of color removal can be achieved, and further stirring till 15 minutes leads to 97% dye color removal.

The process of adsorption is facilitated by various factors including, high surface area, high surface charge, and the presence of compatible functional groups. As evident from results obtained from BET study and zeta potential calculation, surface immobilization by BTCA group on to the Fe_3O_4 NPs led to a significant increase in both surface area and surface charge. Besides these, under synthetic conditions (pH 9–10), the presence of BTCA groups on the Fe_3O_4 surface provides lots of free carboxylate groups ($-COO^-$) covering the surface of Fe_3O_4. During interaction of Fe_3O_4@BTCA and C.R dye, the free carboxylate groups facilitate the adsorption process through formation of a strong H-bond with free $-NH_2$ groups of C.R dye as depicted in Fig. 1, leading to the formation of Fe_3O_4@BTCA@C.R. The involvement of H-bond in the formation of Fe_3O_4@BTCA@C.R is supported by the fact that the asymmetric C-O stretching of carboxylate groups in Fe_3O_4@BTCA at 1581 cm^{-1} almost disappears in Fe_3O_4@BTCA@C.R (Fig. S7 in ESI).

As strong H-bonding plays a crucial role in the adsorption of C.R dye on Fe_3O_4@BTCA, adsorption capacity should drastically decrease in the absence of a strong H-bonding. To confirm this, the free carboxylate groups ($-COO^-$) on Fe_3O_4@BTCA were re-protonated to convert them all to corresponding carboxylic acid ($-COOH$), whose H-bond acceptor ability is much less than the carboxylate groups. When acidified Fe_3O_4@BTCA was subjected to C.R dye adsorption under similar conditions, the observed percentage of color removal was 33% only (Fig. 7). This is also supported by the calculation of zeta potential at various pH (Fig. S3 in ESI), which suggests that in acidic conditions (till pH 5), material bears a positive surface charge. The observation of 33% color removal can be attributed to the fact that under acidic conditions, free $-NH_2$ of the dye will also be converted to $-NH_3^+$ having stronger H-bond donor character than $-NH_2$.

The observation of significantly lowered adsorption capacity of acidified Fe_3O_4@BTCA for C.R dye also corroborates that involvement of H-bonding, owing to the presence of BTCA groups on the Fe_3O_4 surface, is an important factor responsible for unexpectedly high adsorption capacity of Fe_3O_4@BTCA material. In the case of Methyl orange and Crystal violet, however, such H-bonding is not possible because of the unavailability of amine hydrogen atoms due to the presence of tertiary amines in both dyes. Therefore, no appreciable color change is observed when M.O and C.R dye solutions are shaken with Fe_3O_4@BTCA (Fig. S9 in ESI).

In order to perform efficient pollutant sequestration through adsorption, the sorbent should have the ability to be recycled without undergoing any considerable reduction in its adsorption capacity. To investigate such features in our system, the reusability test of Fe_3O_4@BTCA was studied for five cycles by adsorption/desorption and regeneration. The adsorption study was performed by recording the UV-Vis spectra of the remaining filtrate after completion of adsorption in each cycle. The UV-Vis spectra recorded for each cycle is shown in Fig. 8A, and the corresponding percentage color removal ability is represented by a bar diagram in Fig. 8B. From Fig. 8A,B, it
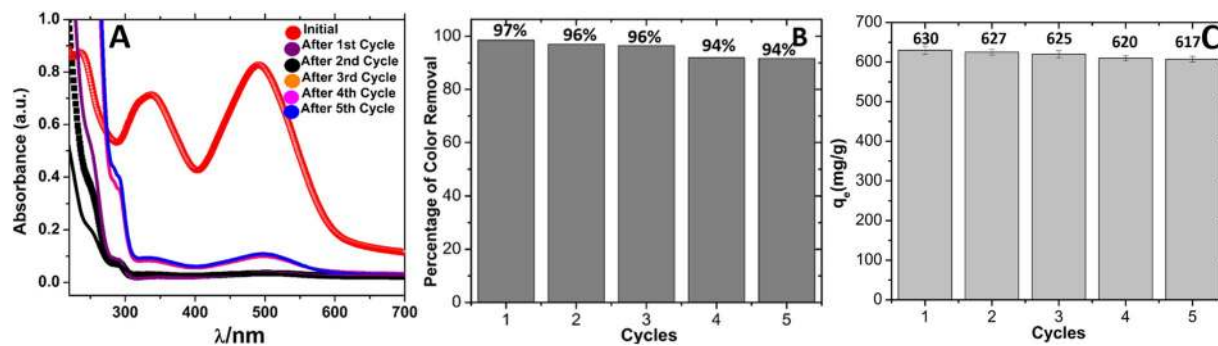
Figure 8. (**A**) UV-Vis Spectra of C.R dye solution after several cycles, (**B**) Percentage of color removal of C.R dye after several cycles, (**C**) Adsorption capacity of Fe_3O_4@BTCA material in five cycles.

is clear that no appreciable reduction (only ~3%) in percentage color removal ability Fe_3O_4@BTCA was observed in five cycles. We also calculated the change in adsorption capacity of our material by performing a batch experiment for each cycle. The values of adsorption capacity for each cycle are given in Fig. 8C as a bar diagram, which shows that, in five cycles, the adsorption capacity of our material is reduced by 2% only. Separation of C.R dye loaded Fe_3O_4@BTCA from aqueous dye solution by magnet is shown in Fig. S10 in ESI.

Conclusion

A new Fe_3O_4@BTCA material has been synthesized by surface functionalization of Fe_3O_4 NPs with 1,2,4,5-Benzenetetracarboxylic acid for rapid and selective adsorption of Congo red dye in an aqueous medium. Adsorption studies show that the Fe_3O_4@BTCA material exhibits high adsorption capacity for C.R dye (630 mg/g) and can be reused for multiple adsorption-desorption cycles without undergoing any considerable loss in its performance. Adsorption isotherm and kinetics studies reveal that the adsorption of C.R dye on the Fe_3O_4@BTCA surface takes place by the Langmuir adsorption model and follows pseudo-second-order adsorption kinetics.

The high adsorption capacity, selectivity and better recyclability of the material can be attributed to surface functionalization ligand BTCA, which, owing to its four uniquely positioned carboxylate group, offers strong surface encourage and participates in the formation of a strong H-bonding only with Congo red dye, containing a primary amine group. This report opens up new possibilities for 1,2,4,5-Benzenetetracarboxylic acid to be explored for surface functionalization of other materials to achieve improved targeted applications.

Experimental Section

Materials. All reagents and chemical used were of analytical standards. In all experiments, double distilled-deionized water was used. $FeCl_3.6H_2O$ (98%), $FeCl_2.4H_2O$ (99%) and 1,2,4,5-Benzenetetracarboxylic acid (BTCA) were purchased from Sigma Aldrich. Ammonia solution (25%), HCl, Congo Red (C.R), Methyl Orange (M.O), and Crystal Violet (C.V) were purchased from Spectrochem. pH buffer tablets were purchased from SRL.

Synthesis of Fe_3O_4 nanoparticles. Fe_3O_4 nanoparticles were synthesized by chemical co-precipitation method[51]. Initially, $FeCl_3.6H_2O$ (5.46 g, 20 mmol) and $FeCl_2.4H_2O$ (2 g, 10 mmol) were dissolved in 400 mL deionized water and kept at room temperature for 15 min with vigorous stirring under a nitrogen atmosphere. After that, 10 mL of ammonia solution (25%) was added drop by drop into the salt solution, and stirring was continued for another 2 h at 80 °C. The solution was cooled, and solid black particles were magnetically separated and repeatedly washed with Millipore water. The particles were finally dried in a vacuum oven at 70 °C for overnight.

Direct functionalization of 1,2,4,5-Benzenetetracarboxylic acid (BTCA) onto Fe_3O_4 surface. In a direct functionalization procedure, 1 g of Fe_3O_4 was taken in a 500 mL round bottom flask containing 200 mL of deionized water. To this suspension, 2 g BTCA (3.905 mmol) and 5 mL aqueous NH_4OH solution were added until the pH reached 11.0. The suspension was refluxed for 24 h in a nitrogen atmosphere with constant stirring. The resulting Fe_3O_4@BTCA material was separated through magnate and washed thoroughly with deionized water thrice to remove unreacted BTCA. The residue was dried under vacuum at 70 °C for 24 h to give brown colored Fe_3O_4@BTCA material.

Instrumentation. Electronic spectra of suspension were recorded on Varian UV−visible spectrophotometer (Carry 100 Bio). FT-IR spectra (4000–400 cm^{-1}) were collected on a Perkin-Elmer GX spectrophotometer (U.S.A) using KBr disks. The zeta potentials were recorded using a Malvern instrument (Zetasizer, Nano series, Nano-ZS90). Scanning electron microscope (SEM) (Leo series 1430 VP) equipped with INCA was used to determine the morphologies of samples. Transmission electron microscopy (TEM) was performed using a JEOL JEM 2100 microscope. Thermogravimetric analysis (TGA) was done using Mettler Toledo TGA/DSC 1 analyzer. Powder X-ray diffraction (XRD) measurements were conducted on Rigaku smart lab automated multipurpose X-ray diffractometer system with CuKα1 radiation ($\lambda = 1.540593$ Å) in the 2θ range of 20–70° at scanning speed of 3° per minute with 0.01° scan step size. The Brunauer− Emmett−Teller (BET) surface area analysis was conducted on an Autosorb iQ, version 1.11 (Quantachrome Instruments).

UV-visible studies. UV-Vis spectra of Fe_3O_4, Fe_3O_4@BTCA, and Fe_3O_4@BTCA@Dye were recorded using suspension of 1 mg of material with 3 mL of deionized water in 1 cm quartz cuvette within the range of 200–800 nm. The uniform suspension was obtained by shaking quartz cuvette on to a vertex shaker for five minutes before the recording of each spectrum. UV-Vis spectra of dyes were recorded in their aqueous solution in the same wavelength range.

Adsorption study of dye on Fe_3O_4@BTCA surface. Batch adsorption experiments were carried out in an aqueous dye solution to determine several adsorption parameters. Adsorption capacity (Q_e) measurements for Congo red dye were done by taking 5 mg of Fe_3O_4@BTCA material in ten batches of 50 ml aqueous dye solution of different concentration (10 ppm to 100 ppm). Each batch containing a suspension of 5 mg of Fe_3O_4@BTCA in aqueous dye solution was stirred at room temperature for 15 min (pH of dye solutions ~7.4), after which, the concentration of unabsorbed dye was determined from UV-Vis spectrum of the filtrate. All the filtrations were done using a strong magnet. All the adsorption experiments were repeated thrice to remove the experimental error.

Reusability test of Fe_3O_4@BTCA. The reusability experiment of material was done through simple acid-base treatments by UV-visible spectral studies and calculation of adsorption capacity. Initially, adsorption of 10 batches of 50 mL aqueous C.R dye solutions of varying concentrations (10–100 ppm) was allowed on 5 mg Fe_3O_4@BTCA and, as discussed in the previous section, filtrate from each batch was subjected to UV-Vis study to determine the amount of adsorbed C.R dye on the Fe_3O_4@BTCA surface. The magnetically isolated sorbent of each batch was washed thoroughly with deionized water and treated with few drops of 0.1 N HCl under vigorous shaking for 5 min and again filtered magnetically to remove the adsorbed C.R dye. After further washing with deionized water twice, the sorbent was treated with few drops of 0.1 N NH_4OH under vigorous shaking. After filtration and proper washing, the regenerated Fe_3O_4@BTCA was dried overnight in a vacuum oven at 70 °C for reuse. The dried material of each batch was again subjected to the same dye adsorption-desorption cycles through acid-base treatment four times. Adsorption parameter from each cycle was determined from the plot of adsorption isotherm using Eq. 2 discussed later.

Data availability
The datasets generated and analyzed during the current study are included in this article and its supplementary information file and also it is available from the corresponding author on reasonable request.

References
1. Immich, A. P. S., De Souza, A. A. U. & De Souza, S. M. A. G. U. Removal of Remazol Blue RR dye from aqueous solutions with Neem leaves and evaluation of their acute toxicity with *Daphnia magna*. *J. Hazard. Mater.* **164**, 1580–1585 (2009).
2. Afkhami, A. & Moosavi, R. Adsorptive removal of Congo red, a carcinogenic textile dye, from aqueous solutions by maghemite nanoparticles. *J. Hazard. Mater.* **174**, 398–403 (2010).
3. Zhao, X. *et al.* Synthesis and characterization of gadolinium doped cobalt ferrite nanoparticles with enhanced adsorption capability for Congo Red. *Chem. Eng. J.* **250**, 164–174 (2014).
4. Lu, L. *et al.* Synthesis of novel hierarchically porous Fe_3O_4@MgAl–LDH magnetic microspheres and its superb adsorption properties of dye from water. *Ind. Eng. Chem. Res.* **46**, 315–323 (2017).
5. Hai, F. I., Yamamoto, K. & Fukushi, K. Hybrid treatment systems for dye wastewater. *Crit. Rev. Environ. Sci. Technol.* **37**, 315–377 (2007).
6. Liu, D., Lei, W., Qin, S. & Chen, Y. Template-free synthesis of functional 3D BN architecture for removal of dyes from water. *Sci. Rep.* **4**, 44–53 (2015).
7. Sinha, A. K., Pradhan, M., Sarkar, S. & Pal, T. Large-Scale Solid-State Synthesis of $Sn–SnO_2$ Nanoparticles from Layered SnO by Sunlight: a Material for Dye Degradation in Water by Photocatalytic Reaction. *Environ. Sci. Technol.* **47**, 2339–2345 (2013).
8. Ihram, M., Guo, C., Guan, Y., Ishfaq, A. & Liu, H. Adsorption and magnetic removal of neutral red dye from aqueous solution using Fe_3O_4 hollow nanospheres. *J. Hazard. Mater.* **181**, 1039–1050 (2010).
9. Sun, H., Cao, L. & Lu, L. Magnetite/reduced graphene oxide nanocomposites: One step solvothermal synthesis and use as a novel platform for removal of dye pollutants. *Nano Res.* **6**, 550–562 (2011).
10. Barragán, B. E., Costa, C. & Márquez, M. C. Biodegradation of azo dyes by bacteria inoculated on solid media. *Dyes Pigments.* **75**, 73–81 (2007).
11. Zaghbani, N., Hafiane, A. & Dhahbi, M. Removal of Safranin T from wastewater using micellar enhanced ultrafiltration. *Desalination* **222**, 348–356 (2008).
12. Paschoal, F. M. M., Anderson, M. A. & Zanoni, M. V. B. The photoelectrocatalytic oxidative treatment of textile wastewater containing disperse dyes. *Desalination* **249**, 1350–1355 (2009).
13. Gupta, V. K., Ali, I., Saleh, T. A., Nayak, A. & Agarwal, S. Chemical treatment technologies for waste-water recycling: an overview. *RSC Adv.* **16**, 6380–6388 (2012).
14. Karthikeyan, S., Gupta, V. K., Boopathy, R., Titus, A. & Sekaran, G. A new approach for the degradation of high concentration of aromatic amine by heterocatalytic Fenton oxidation: kinetic and spectroscopic studies. *J. Mol. Liq.* **173**, 153–163 (2012).
15. Saleh, T. A. & Gupta, V. K. Synthesis and characterization of alumina nano-particles polyamide membrane with enhanced flux rejection performance. *Sep. Purif. Technol.* **89**, 245–251 (2012).
16. Gupta, V. K., Nayak, A. & Agarwal, S. Bioadsorbents for remediation of heavy metals: current status and their future prospects. *Environ. Eng. Res.* **20**, 1–18 (2015).
17. Montalvo, S. *et al.* Application of natural zeolites in anaerobic digestion processes: a review. *Appl. Clay Sci.* **58**, 125–133 (2012).
18. Duman, O., Tunc, S. & Polat, T. G. Adsorptive removal of triarylmethane dye (Basic Red 9) from aqueous solution by sepiolite as effective and low-cost adsorbent. *Microporous Mesoporous Mater.* **210**, 176–184 (2015).
19. Zhu, S., Jiao, S., Liu, Z., Pang, G. & Feng, S. High adsorption capacity for dye removal by CuZn hydroxyl double salts. *Environ. Sci-Nano* **1**, 172–180 (2014).
20. Gouthaman, A., Azarudeen, R. S., Gnanaprakasam, A., Sivakumar, V. M. & Thirumarimurugan, M. Polymeric nanocomposites for the removal of Acid red 52 dye from aqueous solutions: Synthesis, characterization, kinetic and isotherm studies. *Ecotoxicol. Environ. Saf.* **160**, 42–51 (2018).
21. Wang, X. *et al.* Carbon composite lignin-based adsorbents for the adsorption of dyes. *Chemosphere* **206**, 587–596 (2018).

22. Han, X. *et al.* Two-component gelator isomers with different combination of amine and acid: Helical/non-helical morphology and selective adsorption of dyes. *J. Colloid Sci.* **525**, 177–186 (2018).

23. Yan, L. *et al.* An efficient supramolecular adsorbent for co-adsorption of dyes and metal ions from wastewater and its application in self-healing materials. *Soft matter.* **13**, 8772–8780 (2017).

24. Huang, P., Kazlauciunas, A., Menzel, R. & Lin, L. Determining the Mechanism and Efficiency of Industrial Dye Adsorption through Facile Structural Control of Organo-montmorillonite Adsorbents. *ACS Appl. Mater. Interfaces* **9**, 26383–26391 (2017).

25. Jia, Z. *et al.* Synthesis of 3D Hierarchical Porous Iron Oxides for Adsorption of Congo red from Dye Wastewater. *J. Alloys Compd.* **622**, 587–595 (2015).

26. Zhang, Y. *et al.* Selective Adsorption and Separation through Molecular Filtration by Hyperbranched Poly(ether amine)/Carbon Nanotube Ultrathin Membrane. *Langmuir* **32**, 13073–13083 (2016).

27. Chen, X. *et al.* The Synthesis of ZnO/SnO$_2$ Porous Nanofibers for Dye Adsorption and Degradation. *Dalton Trans.* **44**, 3034–3042 (2015).

28. Wu, L., Liu, Y., Zhang, L. & Zhao, L. A green-chemical synthetic route to fabricate a lamellar-structured Co/Co(OH)$_2$ nanocomposite exhibiting a high removal ability for organic dye. *Dalton Trans.* **43**, 5593–5400 (2014).

29. Yavuz, E., Tokalioglu, S. & Patat, S. Core-shell Fe$_3$O$_4$ polydopamine nanoparticles as sorbent for magnetic dispersive solid-phase extraction of copper from food samples. *Food Chem.* **263**, 232–239 (2018).

30. Cui, K. *et al.* Regenerable urchin-like Fe$_3$O$_4$@PDA-Ag hollow microspheres as catalyst and adsorbent for enhanced removal of organic dyes. *J. Hazard. Mater.* **350**, 66–75 (2018).

31. Saksornchai, E., Kavinchan, J., Thongtem, S. & Thongtem, T. Simple wet-chemial synthesis of superparamagnetic CTAB-modified magnetite nanoparticles using as an adsorbent for anionic Congo red dye treatment. *Mater. Lett.* **213**, 138–142 (2018).

32. Saksornchai, E., Kavinchan, J., Thongtem, S. & Thongtem, T. The photocatalytic application of semiconductor stibnite nanostructure synthesized via a simple microwave assisted approach in propylene glycol for degradation of dye pollutants and its optical property. *Nanoscale Res. Lett.* **12**, 589 (2017).

33. Wang, J. *et al.* One-step fabrication of functionalized magnetic adsorbents with large surface area and their adsorption for dye and heavy metal ions. *Dalton Trans.* **43**, 11637–45 (2014).

34. Mollahosseini, A., Toghroli, M. & Kamankesh, M. Zeolite/Fe$_3$O$_4$ as a new sorbent in magnetic solid-phase extraction followed by gas chromatography for determining phthalates in aqueous samples. *J. Sep. Sci.* **38**, 3750–7 (2015).

35. Wang, L., Li, J., Wang, Z., Zhao, L. & Jiang, Q. Low-temperature hydrothermal synthesis of alpha-Fe/Fe$_3$O$_4$ nanocomposite for fast Congo red removal. *Dalton Trans.* **42**, 2572–2579 (2013).

36. Lee, H. U. *et al.* Sea-urchin-like iron oxide nanostructures for water treatment. *J. Hazard. Mater.* **262**, 130–6 (2013).

37. Chaudhary, G. R. *et al.* Adsorption studies of cationic, anionic and azo-dyes via monodispersed Fe$_3$O$_4$ nanoparticles. *J. Nanosci. Nanotechnol.* **13**, 3240–5 (2013).

38. Wang, L., Mao, C., Sui, N., Liu, M. & Yu, W. W. Graphene oxide/ferroferric oxide/polyethylenimine nanocomposites for Congo red adsorption from water. *Environ. Technol.* **38**, 996–1004 (2017).

39. Yan, T. G. & Wang, L. J. Adsorption of C.I. Reactive Red 228 and Congo Red dye from aqueous solution by amino-functionalized Fe$_3$O$_4$ particles: kinetics, equilibrium, and thermodynamics. *Water Sci. Technol.* **69**, 612–621 (2014).

40. Zhao, Y., Chen, H., Li, J. & Chen, C. Hierarchical MWCNTs/Fe$_3$O$_4$/PANI magnetic composite as adsorbent for methyl orange removal. *J. Colloid Sci.* **450**, 189–195 (2015).

41. Yu, L. *et al.* Use of hydroxypropyl-beta-cyclodextrin/polyethylene glycol 400, modified Fe$_3$O$_4$ nanoparticles for congo red removal. *Int. J. Biol. Macromol.* **64**, 233–9 (2014).

42. You, L. *et al.* Facile synthesis of high performance porous magnetic chitosan - polyethylenimine polymer composite for Congo red removal. *Int. J. Biol. Macromol.* **107**, 1620–1628 (2018).

43. Pu, S. *et al.* *In situ* co-precipitation preparation of a superparamagnetic graphene oxide/Fe$_3$O$_4$ nanocomposite as an adsorbent for wastewater purification: synthesis, characterization, kinetics, and isotherm studies. *Environ. Sci. Pollut. Res.* **25**(18), 17310–17320 (2018).

44. Arora, P., Fermah, A., Rajput, J. K., Singh, H. & Badhan, J. Efficient solar light-driven degradation of Congo red with novel Cu-loaded Fe$_3$O$_4$@TiO$_2$ nanoparticles. *Environ. Sci. Pollut. Res.* **24**, 19546–19560 (2017).

45. Li, L., Li, X., Duan, H., Wang, X. & Luo, C. Removal of Congo Red by magnetic mesoporous titanium dioxide-graphene oxide core-shell microspheres for water purification. *Dalton Trans.* **43**, 8431–8438 (2014).

46. Zhu, H. *et al.* Magnetically recyclable Fe$_3$O$_4$/Bi$_2$S$_3$ microspheres for effective removal of Congo red dye by simultaneous adsorption and photocatalytic regeneration. *Sep. Purif. Technol.* **179**, 184–193 (2017).

47. Li, T. *et al.* Synthesis of magnetically recyclable Fe$_3$O$_4$@NiO nanostructures for styrene epoxidation and adsorption application. *Ceram. Int.* **41**, 2214–2220 (2015).

48. Fu, X., Chen, X., Wang, J. & Liu, J. Fabrication of carboxylic functionalized superparamagnetic mesoporous silica microspheres and their application for removal basic dye pollutants from water. *Microporous Mesoporous Mater.* **139**, 8–15 (2011).

49. Qiao, H. *et al.* Effective removal of cationic dyes using carboxylate-functionalized cellulose nanocrystals. *Chemosphere* **141**, 297–303 (2015).

50. He, Y. *et al.* Facile synthesis and functionalization of hyper branched polyglycerol capped magnetic Fe$_3$O$_4$ nanoparticles for efficient dye removal. *Materials Letters* **151**, 100–103 (2015).

51. Alqadami, A. A., Naushad, M., Abdalla, M. A., Khan, M. R. & Alothman, Z. A. Adsorptive Removal of Toxic Dye Using Fe$_3$O$_4$−TSC Nanocomposite: Equilibrium, Kinetic, and Thermodynamic Studies. *J. Chem. Eng. Data* **61**, 3806–3813 (2016).

52. Manna, K. & Srivastava, S. K. Fe$_3$O$_4$@Carbon@Polyaniline Trilaminar Core−Shell Composites as Superior Microwave Absorber in Shielding of Electromagnetic Pollution. *ACS Sustainable Chem. Eng.* **5**, 10710–10721 (2017).

53. Yusoff, A. H. M., Salimi, M. N. & Jamlos, M. F. Synthesis and Characterization of Biocompatible Fe$_3$O$_4$ Nanoparticles at Different pH. *AIP Conference Proceedings* **1835**, 020010–4 (2017).

54. Yan, W. *et al.* Synthesis of Fe$_3$O$_4$ nanoparticles and their magnetic properties. *Procedia Eng.* **27**, 632–637 (2012).

55. Vinosel, V. M., Amaliya, A. P., Vijayalakshmi, S. & Pauline, S. Synthesis and characterization of Fe$_3$O$_4$ nanopowder and dielectric studies. *Int. J. Eng. Res. Appl.* **38**, 17–19 (2016).

56. Oomens, J. & Steill, J. D. Free Carboxylate Stretching Modes. *J. Phys. Chem. A* **112**, 3281–3283 (2008).

57. Guo, H. B., He, F., Gu, B., Liang, L. & Smith, J. C. Time-Dependent Density Functional Theory Assessment of UV Absorption of Benzoic Acid Derivatives. *J. Phys. Chem. A* **116**, 11870–11879 (2012).

58. Chatterjee, S. & Paital, A. R. Functionalized Cubic Mesoporous Silica as a Non-Chemodosimetric Fluorescence Probe and Adsorbent for Selective Detection and Removal of Bisulfite Anion Along with Toxic Metal Ions. *Adv. Funct. Mater.* **28**, 1704726 (2018).

59. Chatterjee, S., Gohil, H. & Paital, A. R. Dual Functions of Selective Ferric ion Detection and Removal by a Recyclable Fluorescence Active Multifunctional Silica Material and Toxic Dye Removal from Aqueous Solution. *Chemistry Select* **2**, 5348–5359 (2017).

60. Hu, J., Wang, X., Liu, L. & Wu, L. A facile and general fabrication method for organic silica hollow spheres and their excellent adsorption properties for heavy metal ions. *J. Mater. Chem. A.* **2**, 19771–19777 (2014).

61. Sun, Z. *et al.* Multifunctional fibrous silica composite with high optical sensing performance and effective removal ability toward Hg^{2+} ions. *J. Mater. Chem. B* **3**, 3201–3210 (2015).

62. Mou, Y., Yang, H. & Xu, Z. Morphology, Surface Layer Evolution, and Structure–Dye Adsorption Relationship of Porous Fe_3O_4 MNPs Prepared by Solvothermal/Gas Generation Process. *ACS Sustainable Chem. Eng.* **5**, 2339–2349 (2017).
63. Giri, S. K., Sahoo, P., Das, R. & Das, N. Coke/Fe_3O_4 nanoparticle composites: synthesis, characterization and adsorption behaviour towards organic dyes. *Desalin. Water Treat.* **57**, 17483–17493 (2016).
64. Tao, H. *et al.* Synthesis of magnetic separable iron oxide/carbon nanocomposites for efficient adsorptive removal of Congo red. *J. Alloy. Comp.* **617**, 76–80 (2014).
65. Guo, R. *et al.* Sandwiched Fe_3O_4/Carboxylate Graphene Oxide Nanostructures Constructed by Layer-by-Layer Assembly for Highly Efficient and Magnetically Recyclable Dye Removal. *ACS Sustainable Chem. Eng.* **6**, 1279–1288 (2018).

Acknowledgements

Author contributions

D.K.R. and S.C. designed the present work. S.C., N.G. and S.K. synthesized the material and performed the dye adsorption studies. D.K.R. and S.C. wrote the paper. A.K.S. and P.M. helped to revise the manuscript.

Competing interests

The authors declare no competing interests.

Additional information

Supplementary information is available for this paper at https://doi.org/10.1038/s41598-019-57017-2.

Correspondence and requests for materials should be addressed to D.K.R.

Reprints and permissions information is available at www.nature.com/reprints.

Publisher's note Springer Nature remains neutral with regard to jurisdictional claims in published maps and institutional affiliations.